8312 *Biochemistry* **2009,** *48,* 8312–8321
DOI: 10.1021/bi900814c

BIOCHEMISTRY
including biophysical chemistry & molecular biology
Article

Occidiofungin, a Unique Antifungal Glycopeptide Produced by a Strain of *Burkholderia contaminans*†

Shi-En Lu,‡ Jan Novak,§ Frank W. Austin,∥ Ganyu Gu,‡ Dayna Ellis,⊥ Marion Kirk,¶ Shawanda Wilson-Stanford,⊥ Marco Tonelli,# and Leif Smith*,⊥

‡*Mississippi State University, Department of Entomology and Department of Plant Pathology, Mississippi State, Mississippi 39762,* §*University of Alabama at Birmingham, Department of Microbiology, Birmingham, Alabama 35294,* ∥*Mississippi State University, College of Veterinary Medicine, Department of Pathobiology and Population Medicine, Mississippi State, Mississippi 39762,* ⊥*Mississippi State University, Department of Biological Sciences, Mississippi State, Mississippi 39762,* ¶*University of Alabama at Birmingham, Comprehensive Cancer Center Mass Spectrometry Shared Facility, Birmingham, Alabama 35294, and* #*University of Wisconsin-Madison, National Magnetic Resonance Facility at Madison (NMRFAM), Madison, Wisconsin 53706*

Received May 11, 2009; Revised Manuscript Received July 27, 2009

ABSTRACT: Bacterial strain *Burkholderia contaminans* MS14 was isolated from soil that suppressed brown patch disease of lawn grass. An antifungal compound was purified from the liquid culture of this bacterium. In this study, complete covalent structures of two purified closely related antifungal compounds were determined by the experiments of TOCSY, NOESY, ROESY, ^{13}C HSQC 2D NMR, and ESI-MS and GC. The analysis of monoisotopic masses of the purified preparation indicated the presence of two related compounds with masses determined to be 1199.543 and 1215.518 Da; the difference corresponds to the mass of an oxygen atom. GC analysis identified a xylose sugar attached to the antifungal compound. NMR experiments revealed that the compound is cyclic and composed of eight amino acids, two of which are β-hydroxy derivatives of Tyr and Asn, and one being a novel amino acid. The novel amino acid serves as the scaffold for the attachment of the xylose and a short acyl chain. The spectrum and concentration of antifungal activity were determined using a microtiter plate assay. The antifungal compound demonstrated potent antifungal activities against a broad panel of fungal plant and animal pathogens, as well as two *Pythium* spp. Microscopic observations showed that the antifungal compound disrupts normal membrane morphology. The cells fill with large inclusion bodies and the membrane becomes irregularly shaped and swollen following the exposure to subinhibitory concentrations of the antifungal compound. Our data support the identification of a novel fungicide and the compound has been named occidiofungin, meaning fungal killer.

Burkholderia contaminans strain MS14 was previously isolated from disease-suppressive soil, a soil in which the soil-borne pathogen causes little or no damage to the host plant (*1*). Initial characterization of this strain showed that it inhibited the growth of a broad range of fungal pathogens (*2*). Subsequently, transposon mutagenesis identified the genomic region responsible for the antifungal activity (*3*), and a 45.2-kb genetic DNA fragment was sequenced and deposited into GenBank with the accession number: EU938698 (*3*, *4*). This genomic region contains several open reading frames, some of which encode regulatory proteins, a cyclic peptide transporter, a glycosyltransferase, a transaminase, and nonribosomal peptide synthetase (NRPS)[1] catalytic modules. The antifungal compound was then isolated and amino acid analysis confirmed that the backbone of the antifungal compound is an oligopeptide that is synthesized via a NRPS mechanism (*3*).

There is a growing demand for new antifungals, given the increasing prevalence of pathogens resistant to current antifungal agents. There are four major therapeutic groups of antifungal agents: polyene antifungals, azole antifungals, allylamine antifungals, and the echinocandins. The first three groups primarily target ergosterol production or bind to ergosterol, disrupting the fungal membrane (*5*−*7*). Ergosterol, much like cholesterol found in mammalian cells, is important for maintaining proper cell permeability and fluidity. The echinocandins, the fourth group, are synthetically modified lipopeptides that originate from the natural compound echinocandin B produced by *Aspergillus rugulovalvus* (*8*, *9*). In fungi, two covalently cross-linked polysaccharides,

†This research was supported in part by the Special Research Initiative of Mississippi Agricultural and Forestry, NMR Facility at the University of Alabama; NIH/NCRR Grant 1S10RR021064-01A1, and the NCI Grant 5P30CA13148, as well as grant support of the National Magnetic Resonance Facility at Madison, which is supported by NIH Grants P41RR02301 (BRTP/ NCRR) and P41GM66326 (NIGMS). Additional equipment was purchased with funds from the University of Wisconsin, the NIH (RR02781, RR08438), the NSF (DMB-8415048, OIA-9977486, BIR-9214394), and the USDA. Funds for the purchase of the mass spectrometers at UAB were obtained from National Institutes of Health/NCRR Shared Instrumentation Grant Awards RR06487 and RR13795. Operation of the Mass Spectrometry Shared Facility is supported by NCI Core Support Grant P30 CA13148 to the University of Alabama at Birmingham Comprehensive Cancer Center.

*To whom correspondence should be addressed. E-mail: jls859@msstate.edu. Fax: (662) 325-7939. Phone: (662) 325-1244.

[1]Abbreviations: NMR, nuclear magnetic resonance; NOE, nuclear Overhauser effect; NOESY, nuclear Overhauser enhancement spectroscopy; TOCSY, total correlation spectroscopy; ROESY, rotational frame nuclear Overhauser effect spectroscopy; HSQC, heteronuclear single quantum coherence; ESI-MS, electrospray ionization mass spectrometry; MS/MS, tandem mass spectrometry; GC, gas chromatography; NRPS, nonribosomal peptide synthetases; NAA, novel amino acid; BHT, β-hydroxy tyrosine; BHN, β-hydroxy asparagine; MIC, minimum inhibitory concentration.

 Published on Web 07/29/2009

(1,3)-β-glucan and chitin, form the primary scaffold that is responsible for the structural integrity and shape of the cell wall (*10*−*13*). The echinocandin class of antifungal agents inhibits (1,3)-β-glucan synthase, an enzyme complex that polymerizes uridine diphosphate glucose into (1,3)-β-glucan polymers (*14*).

A striking feature of some strains of *Burkholderia* is production of various antifungal compounds, which make the organism potentially useful for management of fungal diseases (*15*). However, isolation of *Burkholderia* spp. from cystic fibrosis patients reclassified them as opportunistic pathogens, consequently preventing the direct use of the bacteria for fungal disease management (*16*). Isolation and identification of antifungals responsible for the observed plant-disease suppression activities of the *Burkholderia* strains will provide important avenues for the development of biological-based fungicides, while eliminating potential health risks from using the bacteria directly.

Novel antifungals are needed because of the importance of fungal infections in immunocompromised patients, and the limitations of currently available antifungal agents regarding their spectra of activity and toxicities. In addition, new antifungals are crucial for food preservation and production of a sufficient and affordable food supply. In this study, we characterize the structure and activity of a new antifungal compound named occidiofungin, meaning fungal killer. The complete covalent structure of the antifungal has been elucidated by TOCSY, NOESY, ROESY, and HSQC 2D NMR spectroscopy experiments. Occidiofungin's antifungal activity against a variety of animal and fungal pathogens has been tested. Additionally, aberrant membrane morphology, similar to what has been reported for echinocandins class of antifungals (*17*−*20*), was observed following exposure to sublethal concentrations of occidiofungin, suggesting that occidiofungin also targets the cell envelope. This work provides a substantial base for future experiments aimed at understanding the compound's mode of action, as well as investigating occidiofungin's pharmaceutical and agricultural potential.

EXPERIMENTAL PROCEDURES

All chemicals were purchased from Sigma (St. Louis, MO) and were the highest grade, unless otherwise stated. Occidiofungin was produced and purified as previously described (*3*).

Mass Spectrometry. The antifungal compounds in the active fractions were analyzed by electrospray mass spectrometry (ESI-MS) using a Micromass Q-TOF II mass spectrometer. The compounds were dissolved in 50/50 acetonitrile/water (v/v) with 0.1% formic acid and injected into a 1 μL/min flow of the same solvent using a Harvard syringe pump. The flow was sprayed using the nano-LC interface. Tandem MS (MS/MS) was performed with singly charged ions using standard collision energy (34 V) and higher collision energy (50 V).

Monosaccharide Compositional Analysis. The monosaccharide in the purified occidiofungin was determined as trifluoroacetate of methylglycoside by gas−liquid chromatography (*21*, *22*). The analyses were performed with a gas chromatograph (model 5890, Hewlett-Packard, Sacramento, CA) equipped with a 25-m fused silica (0.22-mm inner diameter) OV-1701 WCOT column (Chrompack, Bridgewater, NJ) and electron capture detector. Sugar standards (pentoses, hexoses, *N*-acetylaminohexoses) were processed at the same time as the test compounds, and the sugar in occidiofungin was determined based on comparison of its chromatographic profile with those of the standards. Sorbitol was used as the internal standard.

NMR Spectroscopy. Occidiofungin is not soluble in aqueous solutions at concentrations required for NMR. Therefore, 5 mM samples of occidiofungin were prepared in 50% acetonitrile-d_3 (Cambridge Isotopes) and 50% water in a total volume of 700 μL. The NMR data were collected on Varian NMR System with Cold Probe spectrometer, operating at a proton frequency of 800 MHz. The ^{1}H resonances were assigned according to standard methods (*23*) using TOCSY (*24*) and NOESY (*25*) experiments. ROESY (*26*) and ^{13}C-HSQC (*27*) experiments were used to clarify some areas of ambiguity in the TOCSY and NOESY spectra. TOCSY, NOESY, and ^{13}C HSQC NMR experiments were collected at 25 °C and the ROESY experiment was collected at 4 °C. The carrier frequency was centered on the water resonance, which was suppressed using the very efficient double-pulsed field gradient selective echo technique (*28*, *29*). A 1.5 s relaxation delay was used between scans. The TOCSY experiment was acquired with a 60 ms mixing time using the DIPSI-2 sequence (*30*). The NOESY and ROESY experiments were acquired with 400 and 100 ms mixing times, respectively. The parameters for collecting the HSQC spectrum were optimized to observe aliphatic CH groups (transfer delay time adjusted for a 140 Hz coupling constant and ^{13}C offset set to 35 ppm). The spectral sweep width for the TOCSY, NOESY, and ROESY was 9000 Hz (11.25 ppm) in both dimensions. The spectral sweep widths for HSQC were 9000.0 Hz (11.25 ppm) in the proton dimensions and 21 200.0 Hz (105.5 ppm) for the carbon dimension. All 2D data were collected with 8192 complex points in the acquisition dimension and between 320 and 512 complex points for the indirect dimensions, except for the HSQC which was collected with 1024 and 192 complex points in the direct and indirect dimension, respectively. Phase sensitive indirect detection for NOESY, ROESY, and TOCSY experiments was achieved using the method of States-TPPI (*31*). A gradient-selected sensitivity-enhanced pulse sequence was used for collecting the HSQC spectrum (*32*, *33*). ^{1}H chemical shifts were referenced to acetonitrile (1.93 ppm). Data were processed with NMRpipe (*34*) by first removing the residual water signal by deconvolution, multiplying the data in both dimensions by a squared cosine function or a squared cosine function with a 608 shift (for the ^{1}H dimension of HSQC), zerofilling once, Fourier transformation, and baseline correction. Data were analyzed with the interactive computer program NMRView (*35*). The NOE cross-peak intensities were measured in NMRView. Distances were calibrated using the relationship $r_{ab}^6 = r_{cal}^6(V_{cal}/V_{ab})$, where r_{ab} is the distance between atoms a and b, V_{ab} is the NOESY a to b cross-peak volume, r_{cal} is a known distance, and V_{cal} is the corresponding volume of the NOESY calibration cross-peak. The distance used for calibrations was the β-hydroxy Tyr4 H^δ and H^ε aromatic protons (2.46 Å).

Microbial Organisms. Fungal strains were obtained from collections at Mississippi State University's Veterinary Medical Research and Diagnostic Laboratory System and Entomology and Plant Pathology Department or were purchased from the American type Culture Collection (Manassas, Va.). Fungal isolates used in this study were *Alternaria alternata, Aspergillus fumigatus, Aspergillus niger, Fusarium oxysporum* f. sp. *lycopersici* ATCC9848, *Geotrichum candidum* F-260 (*36*), *Macrophomina*

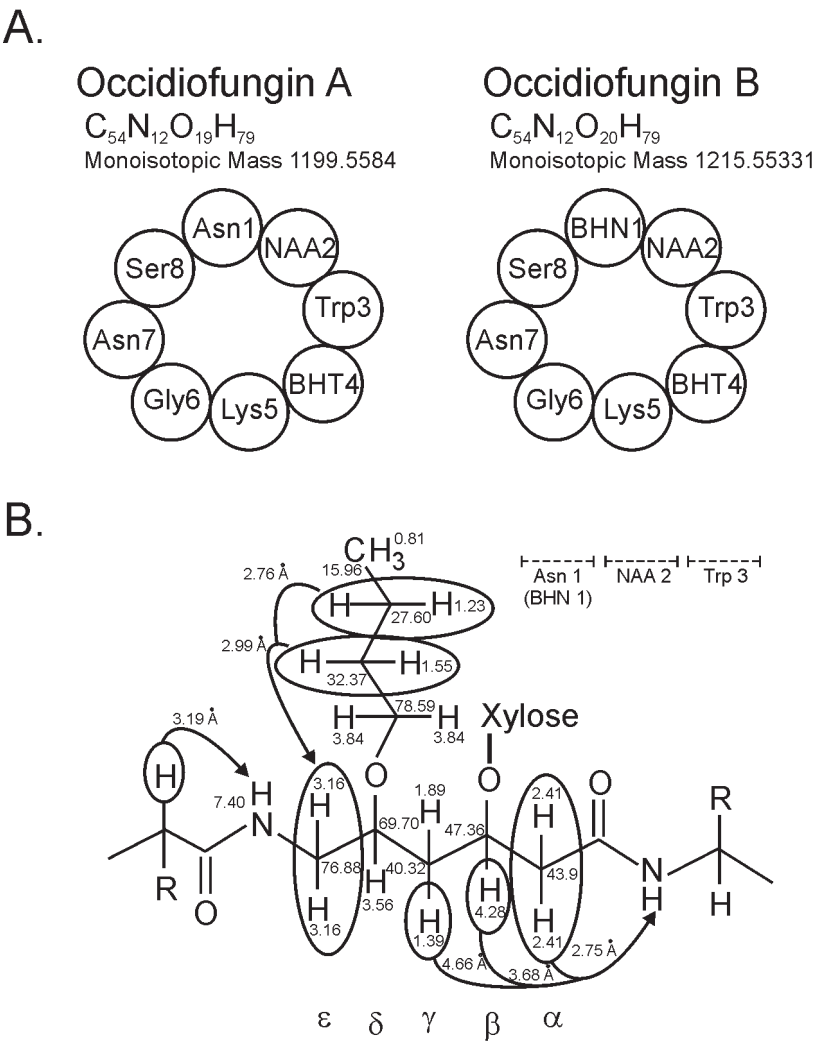

FIGURE 1: Covalent structure of occidiofungin. In panel A, representative structures of occidiofungin A and occidiofungin B are shown. In panel B, a representative structure of novel amino acid 2 is shown. The chemical shift values (in ppm) are shown next to their respective atoms. NOE values are written next to the circles and arrows designate the proton interactions.

phaseolina 61 (from Dr. Richard Baird), *Microsporum gypseum, Penicillium* sp., *Rhizoctonia solani* MSCOT-1, and *Trichophyton mentagrophytes*. In addition, two *Pythium* species (from Dr. David Ingram) were tested: *Pythium spinosum* 472-04 and *Pythium ultimum* 671-04.

Antifungal Susceptibility Testing. Minimum inhibitory concentrations were determined by agar microdilution testing. Occidiofungin was serially 2-fold diluted (32 μg/mL to 62.5 ng/mL) with sterile water and was added to flat bottomed 12-well plates. One milliliter of Sabouraud dextrose agar Difco (BD Diagnostics, Franklin Lakes, NJ) was added to each well. Once the agar solidified, the plates were stored inverted at 4 °C until used. Fungal cultures were grown on 100 × 15 mm Sabouraud dextrose agar plates (Thermo Fisher Scientific Remel Products, Lenexa, KS) at 22 °C for 7 days. A circular punch, containing a 1 cm in diameter plug of the fungi from the agar plate, was made from an area of the plate having a confluent growth of the fungi. The plug was placed in 3 mL of PBS and ground with approximately 30 strokes of a Ten-brock homogenizer. Five microliters of the supernatant was placed in the center of each well and allowed to dry before incubating the microtiter plates at 22 °C. Minimum inhibitory concentrations were measured at 48 h for each species, except for *T. mentagrophytes*, which was measured at 72 h. MICs were determined as the lowest concentration that inhibited visible fungal growth. MIC_{50} values were determined as a concentration that visibly reduced colony growth by more than 50% (in diameter) as compared to the control.

Microscopy. The fungi growing in flat-bottomed 12-well plates described above were used for examination of the effects of occidiofungin on the fungal hyphae and arthrospores. For each of the fungi, the hyphae or arthrospores with an observed MIC_{50} at 48 h growing next to the MIC well were used for preparation of light microscopy and transmission electron microscopy (TEM) slides. For light microscopy, lactophenol cotton blue solution was used as a positive stain and mounting medium for the slide. For TEM, the *G. candidum* samples were fixed at 4 °C with 2.5% glutaraldehyde in 0.1 M phosphate buffer (pH 7.2). After being rinsed with the buffer, specimens were postfixed with 2% osmium tetroxide in the phosphate buffer. The specimens washed with the phosphate buffer were dehydrated in graded ethanol serials (50−100%), and then embedded in Spurr's resin. Thin sections generated with a Reichert-Jung Ultracut E Ultramicrotome (60−90 nm) were double stained with uranyl acetate and lead citrate as described previously (*37*). The grids were observed under a transmission electron microscope Jeol JEM-100CXII (Joel Ltd., Tokyo, Japan). Images were taken at magnifications between 5000 and 8000.

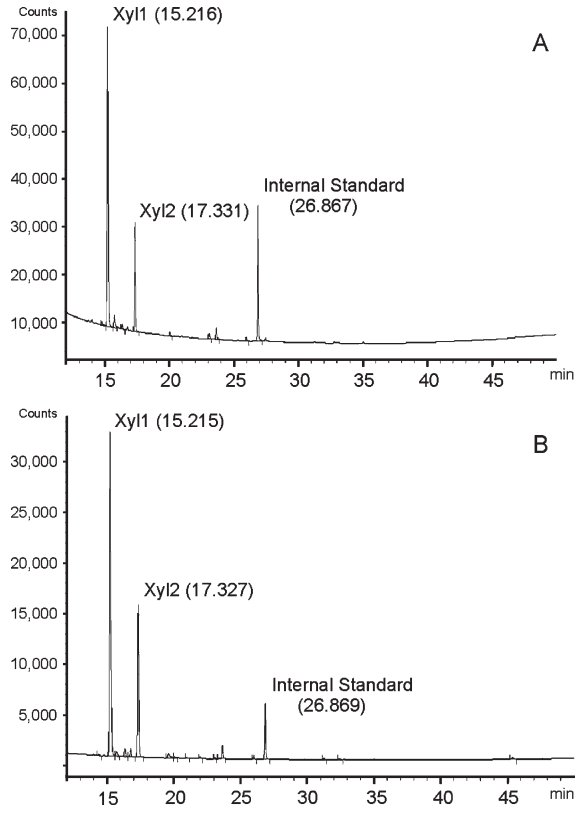

FIGURE 2: GC chromatograms of a standard of xylose (A) and the glycan from occidiofungin (B); internal standard was added to both samples. Xylose standard showed two peaks (Xyl1 and Xyl2); occidiofungin glycan was identified as xylose based on the identical migration times of both peaks (shown in parentheses in the figure).

RESULTS

Occidiofungin is a Cyclic Glycopeptide. High-resolution mass spectrometry data revealed the existence of two structural variants of the antifungal peptide; one having a monoisotopic mass of 1199.543 Da and the other having a monoisotopic mass of 1215.518 Da which corresponds to the addition of oxygen to the first compound. These masses are in accordance with the elucidated structure (calculated monoisotopic masses of 1199.5584 and 1215.5533) shown in Figure 1. Given the presence of two structural variants, the variants of the antifungal compound are referred to as occidiofungin A (1199.5584 Da) and occidiofungin B (1215.5533 Da). ESI-TOF MS/MS analysis of the antifungal compound was inconclusive, as the standard collision energy resulted only in the loss of glycan and the high collision energy that was required to fragment the antifungal compound produced a complex series of daughter ions. However, the fact that high energy of dissociation was required for fragmentation to occur suggests that the compound is a cyclic peptide (*38*, *39*). A standard dissociation method resulted only in a loss of 149 Da from the parental ion, indicating the presence of a pentose sugar. GC analysis revealed that the sugar attached to the oligopeptide is a xylose (Figure 2). As previously reported, amino acid analysis revealed the presence of a lysine (*3*). However, attempts to digest the peptide with trypsin were unsuccessful, presumably due to the specific structural characteristics of the compound (data not shown). Failure to linearize the antifungal peptide prevented subsequent ESI-MS analysis.

NMR proved to be the definitive method for determining the structure of the antifungal oligopeptide. To determine the complete covalent structure of the antifungal peptide, we collected TOCSY, NOESY, ROESY, and HSQC data. The TOCSY and NOESY data sets provided unambiguous sequential assignments, and the ROESY and HSQC data set was used as supporting evidence to the proton-based assignments. TOCSY/NOESY data sets revealed the presence of 13 distinct spin systems in the amide proton frequency of the spectrum. This number of spin systems is more than expected for an oligopeptide with a mass of 1199 and 1215 Da. Further analysis of the data set revealed that the oxidized variant, occidiofungin B, has several distinct spin systems in the amide frequency of the TOCSY spectrum (Figure 3A).

Occidiofungin A is composed of an Asn1-novel amino acid 2 (NAA2)-Trp3-β-hydroxy Tyr4-Lys5-Gly6-Asn7-Ser8 (Figure 1A). Numerical assignment of the amino acids is attributed to sequencing data outlining the location of the thioesterase domain in the NRPS complex (*3*); the location of the thioesterase domain typically designates the C-terminus of the oligopeptide (*40*). Residues 1 and 7 of occidiofungin A have a chemical shift pattern characteristic of an Asn residue (Table 1). NAA2 has a chemical shift pattern characteristic of deaminated lysine, with a short acyl group and xylose sugar attached (Figures 1B and 3B). Given the unique characteristics of this residue, its structure is discussed separately below. Residue 3 has a chemical shift pattern characteristic of a Trp residue. NOEs were absent between protons on the indole ring to the beta protons of Trp and to other residues in the compound. This suggests that the tryptophan ring is rotationally unrestrained in the solvent, resulting in a loss of signal due to a conformationally averaged distance greater than 5 Å. Further evidence for solvent accessibility of the tryptophan indole ring comes from the lack of a resonance of the indole NH (epsilon) of Trp. Exchange of the NH proton of indole with the aqueous environment is accelerated when the indole ring is exposed to the solvent under acidic pH, resulting in a loss of signal due to line broadening (*41*). Residue 4 is a modified Tyr residue. The beta carbon is hydroxylated resulting in a remarkable downfield shift of the beta proton to 5.16 ppm. NOEs are observed between the delta protons of the aromatic ring to the beta proton of β-hydroxy Tyr, enabling definitive assignment of the aromatic proton frequencies. Residues 5, 6, and 8 have typical chemical shift patterns for Lys, Gly, and Ser, respectively. Occidiofungin B differs from occidiofungin A in that the β-carbon of Asn1 is hydroxylated, resulting in a β-hydroxy Asn residue at position 1. Hydroxylation of the beta carbon resulted in the beta proton shifting downfield to 4.24 ppm from 2.67 ppm. Furthermore, hydroxylation of beta carbon of Asn1 resulted in noticeable changes in the chemical shifts in the amide proton frequency of the NAA2, Trp3, Asn7, and Ser8, suggesting differences in the overall conformation of occidiofungin A and occidiofungin B. Definitive assignment of all the Asn residues and the β-hydroxy Asn residue in the antifungal compound came from the ROESY data set in which ROEs from the beta protons to the delta protons of the amino group were observed (Supporting Information, Figure S1).

Residues 1 through 8 of occidiofungin A and occidiofungin B were sequentially assigned through an H^{α}_{i} and H^{β}_{i} to H^{N}_{i+1} sequential walk. NOE connectivities are shown in red in Figure 4 for occidiofungin A and occidiofungin B. A complete sequential walk could be done for both variants of occidiofungin. NOEs exist between H^{α} and H^{β} of Asn1 and the H^{α} of β-hydroxy Asn1 to H^{N} of the NAA2 of each variant. NOEs exist between H^{α}, H^{β}, and H^{γ} of NAA2 to H^{N} of Trp3 of each variant. Trp3 has an H^{α}

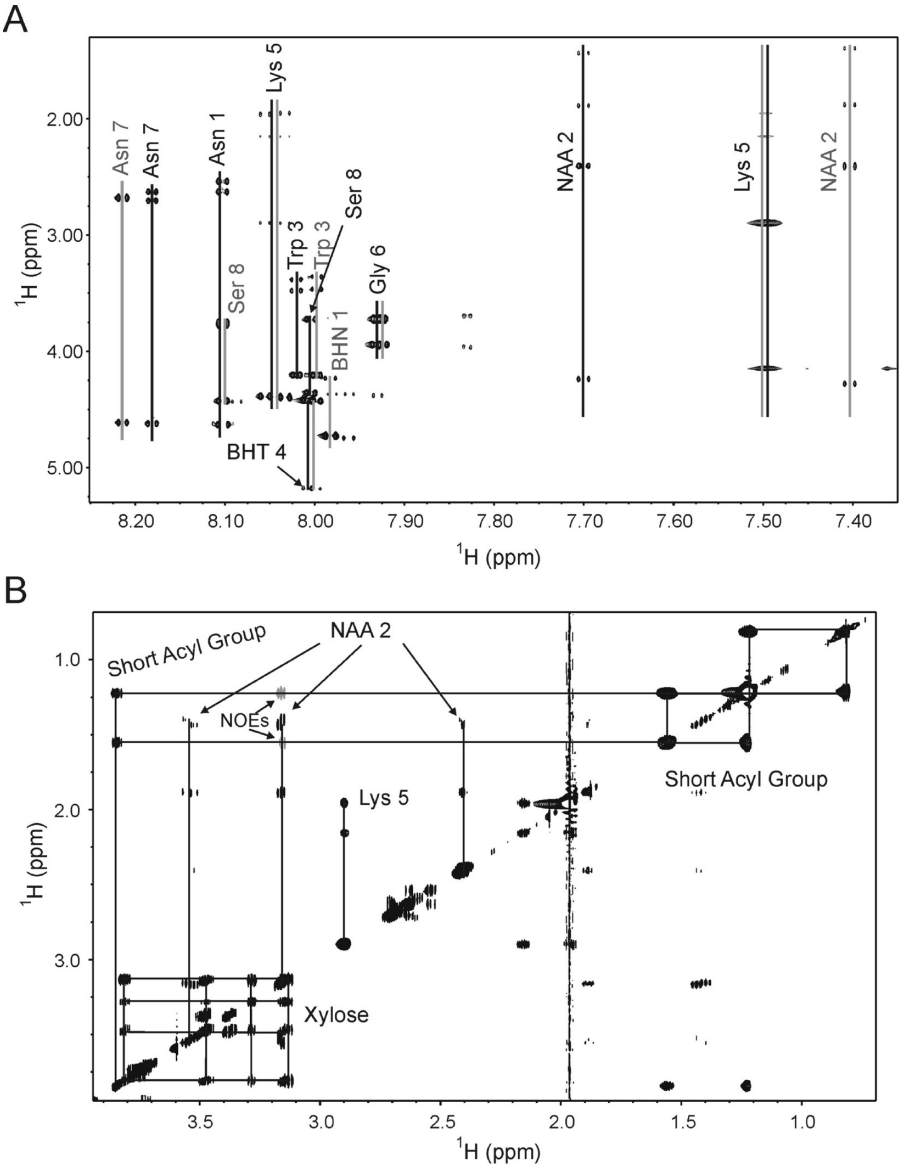

FIGURE 3: TOCSY and NOESY NMR spectra of occidiofungin. In panel A, expansion of the TOCSY 2D NMR spectra showing the amide to alpha, and amide to side chain spin systems for each assigned residue in occidiofungin A (black) and occidiofungin B (gray). In panel B, expansion of the NOESY 2D NMR spectra showing the chemical shifts of the short acyl group and xylose sugar in occidiofungin. NOEs (colored in gray) between the protons of acyl carbons 2 and 3 and the H^{ϵ} proton of the NAA are differentiated by arrows.

proton NOE to H^N of β-hydroxy Tyr4. NOEs exist between H^{α} and H^{β} of β-hydroxy Tyr4 and Lys5 to H^N of Lys5 and Gly6, respectively. Gly6 has an H^{α} proton NOE to H^N of Asn7 of each variant. Additional NOEs exist between H^{α} and H^{β} of Asn7 and H^N of Ser8 of each variant. Furthermore, evidence of the cyclic nature of the oligopeptide comes from NOEs between H^{α} of Ser8 of occidiofungin A and H^{α} and H^{β} of Ser8 of occidiofungin B to H^N of Asn1 and H^N of β-hydroxy Asn1, respectively. $H^N{}_i$ to $H^N{}_{i+1}$ NOEs were observed between NAA2 to Trp3, Lys5 to Gly6, Gly6 to Asn7, and Asn 7 to Ser8 for both occidiofungin A and occidiofungin B (Supporting Information, Figure S2). Additional $H^N{}_i$ to $H^N{}_{i+1}$ NOEs were observed between Asn1 to NAA2 and β-hydroxy Asn1 to NAA2 for occidiofungin A and occidiofungin B, respectively.

Because of the unique structure, a schematic of residue 2 is provided in Figure 1B. The structural base of NAA2 is similar to a deaminated lysine. Presumably, this residue is formed by the ketoacyl synthase and transaminase found in the genomic region responsible for the synthesis of the antifungal compound (Gu, Smith, and Lu, unpublished). Using the elemental assignments of a deaminated lysine as reference, the chemical shift assignments for the alpha, beta, gamma, delta, and epsilon protons is supported by NOE data. NOEs between the H^{α}, H^{β}, and H^{γ} of NAA2 to H^N of Trp3 are observed (Figure 4). The intensities of the NOEs decrease as the distances of the protons to the H^N of Trp3 increase (Figure 1B). Furthermore, the terminal amino group on the deaminated lysine-like residue is covalently linked to the preceding Asn residue's carbonyl group, as observed by the NOEs described above. Analyses of the chemical shifts in this region suggest that the NAA2 provides the base for attaching a four carbon acyl chain and the xylose sugar (Table 1). The data support the attachment of the acyl chain to the delta carbon and attachment of the xylose sugar to the beta carbon of the deaminated lysine-like residue. The predicted chemical shift value for protons on a saturated carbon in this region would be approximately 1.7 ppm. The beta and delta protons are significantly shifted downstream of this predicted value to 4.28 ppm and 3.56 ppm, respectively (Table 1 and Figure 4). The change in

Table 1: Chemical Shifts[a]

amino acid	H^N	H^α	H^β	other proton
Asn 1	8.10	4.62 (53.20)	2.54, 2.63 (39.98)	7.42[b]
BHN 1	7.98	4.73 (58.74)	4.24	7.49[b]
NAA 2		2.41 (43.90)	4.23 (47.36)	1.89 (40.32), 1.44 (40.32), 3.52 (69.70), 3.17 (76.88), 7.67
NAA 2		2.41 (43.90)	4.28 (47.36)	1.89 (40.32), 1.39 (40.32), 3.56 (69.70), 3.16 (75.80), 7.40
Trp 3	8.02	4.20 (58.54)	3.49, 3.39 (64.05)	7.45, 7.04, 7.33, 6.65
Trp 3	8.00	4.20 (58.54)	3.47, 3.35 (64.05)	7.45, 7.04, 7.33, 6.65
BHT 4	8.00	4.42 (63.18)	5.16 (74.06)	7.17, 6.76
Lys 5	8.04	4.39 (53.88)	2.15 (31.29)	1.96 (31.29), 2.90 (39.25), 7.49
Gly 6	7.93	3.94, 3.72 (45.06)		
Asn 7	8.18	4.63 (53.13)	2.70, 2.63 (38.58)	7.41[b]
Asn 7	8.21	4.62 (53.13)	2.67 (38.58)	7.43[b]
Ser 8	8.00	4.35 (58.27)	3.73 (64.24)	
Ser 8	8.10	4.43 (58.27)	3.76 (64.24)	
xylose				4.30, 3.81 (67.90), 3.48 (72.08), 3.28 (78.47), 3.14 (67.92)
acyl chain				3.84 (78.59), 1.55 (32.37), 1.23 (27.60), 0.81 (15.96)

[a] Proton chemical shift values are from a TOCSY experiment. Chemical shifts in parentheses are ^{13}C values from the HSQC experiment. Distinct chemical shift values for occidiofungin B are shown in grey. [b] Indicates chemical shift values from the ROESY experiment.

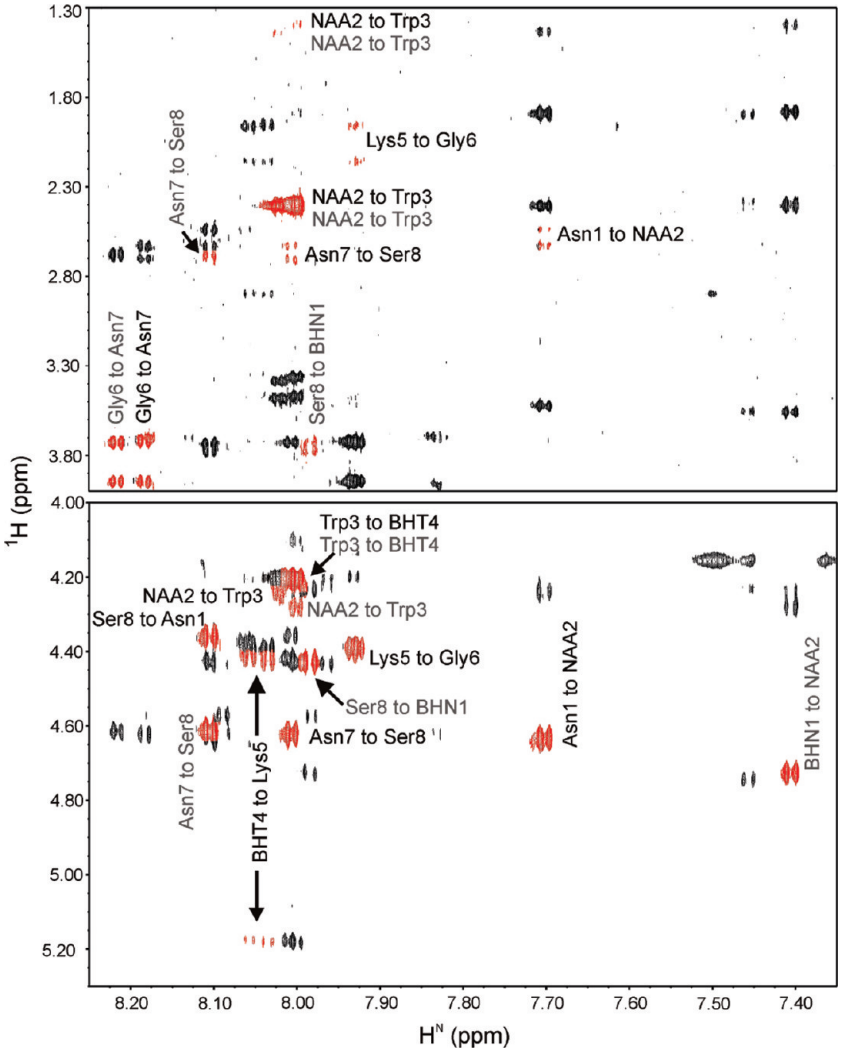

FIGURE 4: NOESY NMR spectra of occidiofungin. The expansion shows the amide to alpha, and amide to side chain interactions. The respective amino acid interactions are labeled next to their inter-residue NOE's shown in red. Residues for occidiofungin A and occidiofungin B are presented in black and gray, respectively.

the chemical shifts of these protons suggests the presence of an electron withdrawing group, such as oxygen in their vicinity. It is predicted that the double bonded oxygen on the delta and beta carbons, which would be present as part of fatty acid synthesis by the ketoacyl synthase, are reduced to a hydroxyl group, and subsequently the four carbon acyl chain and xylose sugar are attached via condensation reaction. NOEs between the protons of acyl carbons 2 and 3 exist to the H^ε proton of the deaminated

A

Organism	MIC (μg/mL)	MIC_{50} (μg/mL)	Pathogen
Alternaria alternata	8	1	Plant and Animal
Aspergillus fumigatus	8	1	Animal
Aspergillus niger	4	0.25	Plant and Animal
Fusarium oxysporum	>32	16	Plant
Geotrichum candidum	8	4	Plant and Animal
Macrophomina phaseolina	2	0.25	Plant
Microsporum gypseum	4	1	Animal
Penicillium sp.	32	16	Plant and Animal
Pythium spinosum	1	0.5	Plant
Pythium ultimum	2	1	Plant
Rhizoctonia solani	2	0.5	Plant
Trichophyton mentagrophytes	4	2	Plant and Animal

B

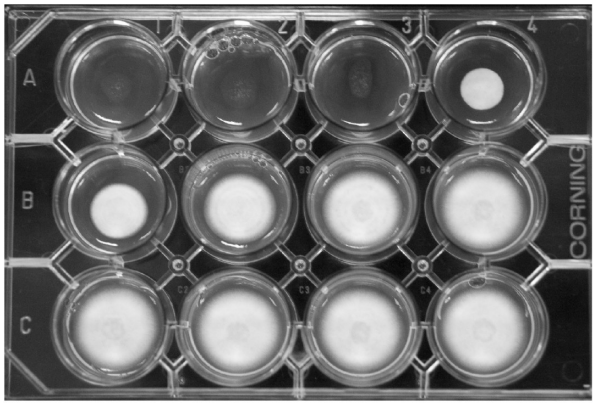

FIGURE 5: Spectrum of activity for occidiofungin. In panel A, MIC values are presented for several plant and animal pathogens. MIC and MIC_{50} represent 100% growth inhibition and >50% growth inhibition, respectively. In panel B, a representative bioassay plate is shown of *Geotrichum candidum*. Serially diluted sample was used, from the initial concentration of 32 μg/mL in well A1 to the lowest concentration of 62.5 ng/mL in well C2. The last two wells serve as a negative control (no antifungal compound). Well A4 is a good representation of a MIC_{50}, in which the growth of the fungus was inhibited by more than 50%.

lysine-like residue (Figures 1B and 3B), supporting the attachment of the acyl group to the delta carbon. The Ser8 residue in the molecule could also support the attachment of the xylose. However, the lack of any notable changes in its predicted chemical shift values adds significance to the dramatic downstream shift of the H^{β} proton observed in NAA2. The attachment of the xylose to other residues in the molecule would result in a loss of oxygen on the xylose molecule, resulting in a lower mass than what was observed in the mass spectrometry data described above. Consequently, the beta carbon of NAA2 is the most plausible attachment site for the xylose. The HSQC data provided additional correlation between the protons of the NAA2 to the carbon resonances of the modified residue. For instance, the carbon resonance for the gamma carbon had two distinguishable protons with resonances of 1.89 and 1.39 ppm (Figure 1 and Supporting Information, Figure S3).

Occidiofungin Has a Broad Spectrum of Antifungal Activity. Occidiofungin demonstrated significant antifungal activity against a broad array of plant and animal fungal pathogens (Figure 5). *R. solani* was the most sensitive of the fungi tested with an MIC of 2 μg/mL and exhibited significant growth inhibition at a concentration of 0.5 μg/mL. *A. fumigatus* and *A. niger*, which are common causes of invasive pulmonary aspergillosis (*42*), both were highly susceptible to occidiofungin with a MIC of 8 μg/mL and 4 μg/mL, respectively. Two fungi, *M. gypseum* and *T. mentagrophytes* which are both associated with dermatophytosis (*43*), were sensitive to occidiofungin with MICs of 4 μg/mL.

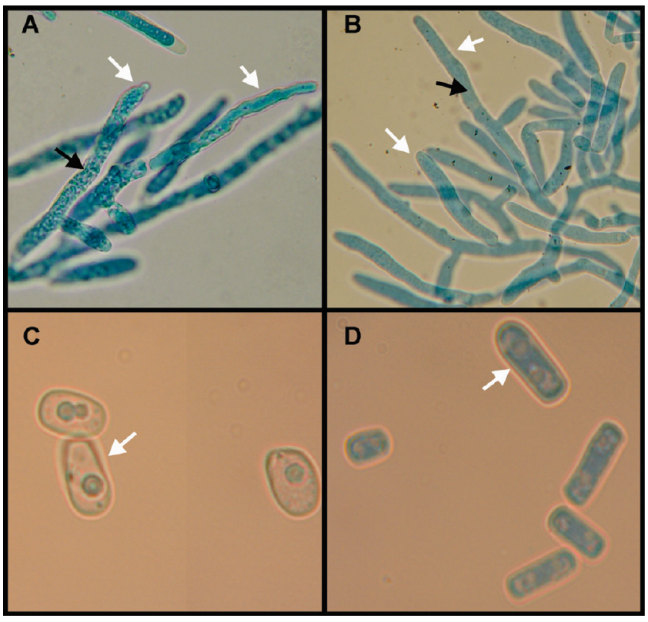

FIGURE 6: Light microscopy. In panels A and B, significant hyphal morphological changes in *Rhizoctonia solani* grown in subinhibitory concentrations (panel A) are notably observed when compared to control (panel B). Black arrows point to the formation of intracellular inclusions and the white arrows point to membrane deformities. In panels C and D, *Geotrichum candidum* exposed to 4 μg/mL of occidiofungin for 48 h (panel C) resulted in significant swelling of the cells, as compared to control (panel D).

Additional pathogenic fungi, *Penicillium* sp., *A. alternata*, and *M. phaseolina*, were shown to be sensitive to occidiofungin with an MIC of 32 μg/mL, 8 μg/mL, and 2 μg/mL, respectively. The fungus *F. oxysporum* was the least sensitive to occidiofungin with a MIC > 32 μg/mL. However, significant growth inhibition was observed at 16 μg/mL. *G. candidum*, a yeast pathogen of plants and animals (*44*, *45*), was significantly inhibited having an MIC of 8 μg/mL and remarkable growth inhibition at 4 μg/mL (Figure 5B). *P. spinosum* and *P. ultimum* were the most sensitive to occidiofungin, with a MIC of 1 μg/mL and 2 μg/mL, respectively. These data indicate that occidiofungin has possible application as a potent broad spectrum antifungal agent against plant and animal fungal pathogens.

Occidiofungin Alters Cell Wall Integrity. Hyphae and cells of equivalent age were used in these studies. Hyphae of *R. solani* growing in subinhibitory concentrations of occidiofungin (0.5 μg/mL) were compared to hyphae of *R. solani* growing in the absence of the antifungal compound. There was more than a 50% reduction in growth of *R. solani* at this concentration (Figure 5A). Occidiofungin induced significant hyphal morphological changes, with one of the most notable changes being the formation of intracellular inclusions (Figure 6A,B, black arrows). Another noticeable difference was the deformation of the tips of the hyphae and the undulated pattern of the cell membrane following exposure to occidiofungin (panel A and B, white arrows). The same observation was made on hyphae morphology of *M. phaseolina* grown under subinhibitory concentrations (not shown). Arthrospores of *G. candidum* exposed to 4 μg/mL of occidiofungin for 48 h showed amorphous shapes due to cellular swelling following exposure (Figure 6C,D) when compared with untreated cells. TEM data shows a dramatic decrease in cell wall thickness of *G. candidum* following exposure to subinhibitory concentrations of occidiofungin for 48 h (Figure 7). In addition,

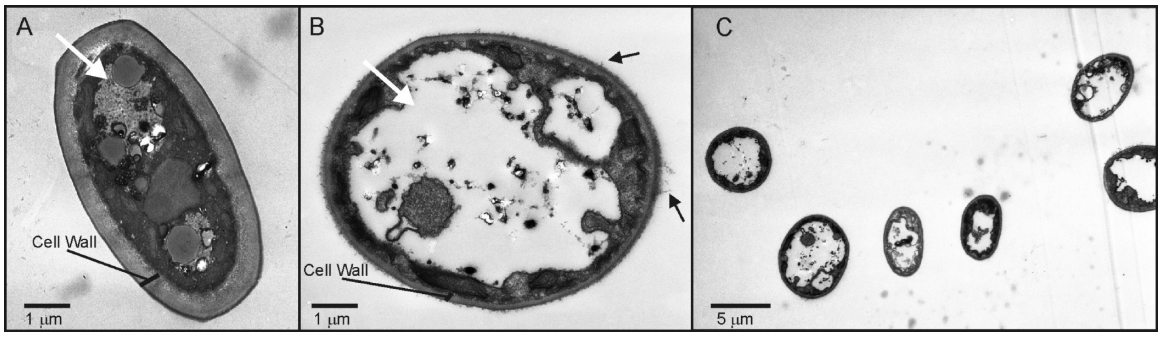

FIGURE 7: Transmission electron microscopy. *Geotrichum candidum* exposed to 4 μg/mL of occidiofungin for 48 h (panel B) resulted in remarkable morphological changes, as compared to control (panel A). Cell wall thickness is drastically reduced compared to control. The exterior cell wall of treated *Geotrichum candidum* appears to be sloughing off (black arrow). The lack of contrast inside the treated cell (white arrow) suggests that the cell has lysed and effluxed cellular components. Panel C shows a wider view containing several arthrospores exposed to occidiofungin. Images in panels A−C were taken at a magnification of 8000.

what appears to be sloughing of the cell wall is present in the treated sample (black arrows), which suggests that cell wall integrity is affected by exposure to occidiofungin. The lack of internal cellular contrast in the treated *G. candidum* also suggests that the cell has lysed (white arrow). Presumably, the thinner cell wall is unable to maintain the osmotic pressure. No statement about swelling can be made from the TEM data, given that the arthrospores are cylindrical and the chance of cross sectioning them is high. A wider view showing several arthrospores does show that some of the arthrospores do retain a cylindrical appearance (Figure 7C), nonetheless, they all share the same morphological deformities internally and in the cell wall as seen in the arthrospore shown in panel B. These observations indicate that occidiofungin targets membrane integrity by disrupting cell wall formation and that occidiofungin may inhibit enzyme function, since the formation of visible inclusion bodies are generally attributed to substrate accumulation.

DISCUSSION

The findings from this study include the elucidation of the complete covalent structure of occidiofungin which contains a novel amino acid; characterization of the broad spectrum antifungal activity of occidiofungin; and in vivo observation of cellular inclusions and membrane instability following exposure to the antifungal compound.

Structural characterization confirms that occidiofungin is a unique antifungal agent. All of the mass spectrometry and NMR data presented above are in complete agreement and support the structure of occidiofungin shown in Figure 1. The structural data provided unambiguous amino acid assignments enabling us to distinguish between the two structural variants of occidiofungin, occidiofungin A and occidiofungin B. A complete sequential walk across the backbone of each molecule was shown. Furthermore, NOEs from the C-terminal residue Ser8 to Asn1 of occidiofungin A and β-hydroxy Asn 1 of occidiofungin B confirm the cyclic nature of the oligopeptide that was predicted previously (*3*).

A novel amino acid was identified and is well characterized by the NMR data. The importance of this unique residue for the antifungal activity is unknown, but is an area of enormous interest by our group. In addition, two amino acid derivatives, β-hydroxy Asn (exclusive to occidiofungin B) and β-hydroxy Tyr were identified in the NMR data (Table 1). Chromatographic separation of each variant has not yet been accomplished. Therefore, it is not yet known if the hydroxylation of the beta carbon of Asn 1 is important for the bioactivity of the compound. The dramatic shift in the amide frequencies of the residues near β-hydroxy Asn 1 does suggest that the conformation of the peptide did change following hydroxylation of the beta carbon of Asn 1.

The exact mechanism of activity of occidiofungin is not known, but this study provides a solid base to begin experiments to elucidate the mechanism of action. Occidiofungin demonstrated strong inhibitory activity against two *Pythium* species. *Pythium* is not a true fungus and ergosterol is not present as a main sterol in their cellular membranes; consequently, it is insensitive to antifungals that target ergosterol (*46*, *47*). Thus, the antifungal activity of occidiofungin presumably does not involve binding ergosterol or inhibiting ergosterol synthesis. It is also important to note that the cell wall of *Pythium* does not contain chitin and that this oomycete contains a great amount of β-glucan in its cell wall. Thus, it is also not likely that occidiofungin targets chitin synthesis.

The morphology of fungi exposed to occidiofungin resembles the morphology reported in the literature of fungi exposed to echinocandins (*17*−*20*), suggesting that occidiofungin may target glucan synthesis. *A. fumigatus* exposed to inhibitory concentrations of micafungin, an echinocandin, displayed hyphal burst (*9*, *19*) and showed undulated membranes and deformed hyphae tips at subinhibitory concentrations (*18*). *Candida albicans* exposed to a lethal dosage of echinocandins induce swelling and at subinhibitory dosage abnormal morphological changes were observed on the membrane (*17*, *20*). The formation of aberrant membrane morphology in *A. fumigatus* is similar to what was observed when *R. solani* and *M. phaseolina* were grown under subinhibitory concentrations and the cellular swelling of *C. albicans* resembles what was observed for *G. candidum* exposed to a subinhibitory dose of occidiofungin.

Interestingly, *Fusarium* spp. are resistant to echinocandins. The mechanism of resistance is attributed to natural mutants in the catalytic subunit of the (1,3)-β-glucan synthase enzyme (*14*) and natural differences in cell wall structure, specifically, *Fusarium* spp. possess less 1,3-β-glucans (*6*, *7*). While the MIC of *F. oxysporum* was >32 μg/mL in this study, occidiofungin dramatically slowed the growth of this fungus at 16 μg/mL. Further studies will explore whether occidiofungin inhibits glucan fungal cell wall synthesis, in particular whether it inhibits (1,3)-β-glucan synthase. Cell wall formation and responses to cell wall damage involve an intricate cell signaling network, which orchestrates communication between the fungal cell wall surface to biosynthetic enzymes for synthesis and repair

(*48*−*50*). Consequently, the exact mechanism of action of occidiofungin could involve a completely novel target.

ACKNOWLEDGMENT

The authors thank Amanda Lawrence, research associate at the Electron Microscopy Facilities at Mississippi State University, for all her help. The authors also gratefully acknowledge the technical assistance with GC and mass spectrometry by Rhubell Brown and Landon Wilson. Lastly, we would like to thank Drs. Richard Baird and David Ingram from Department of Entomology and Plant Pathology at Mississippi State University for their microbial strains.

SUPPORTING INFORMATION AVAILABLE

Figure S1 showing the ROEs from the beta protons to the delta protons of the amino group for Asn1, BHN2, and Asn7, Figure S2 showing the H^N_i to H^N_{i+1} NOEs, and Figure S3 showing the complete assignment of the ^{13}C-HSQC data set. This material is available free of charge via the Internet at http://pubs.acs.org.

REFERENCES

1. Cook, R. R., Baker, K. F. (1983) The Nature and Practice of Biological Control of Plant Pathogens , American Phytopathological Society, St. Paul, MN.
2. Lu, S.-E., Woolfolk, S., and Caceres, J. (2005) Isolation and identification and genetic analysis of rhizobacteria antagonistic to plant soilborne fungal pathogens. *Phytopathology 95*, 62–63.
3. Gu, G. Y., Smith, L., Wang, N., Wang, H., and Lu, S.-E. (2009) Biosynthesis of an antifungal oligopeptide in *Burkholderia contaminans* strain MS14. *Biochem. Biophys. Res. Commun. 380*, 328–332.
4. Gu, G., Wang, N., Chaney, N., Smith, L., and Lu, S.-E. (2009) AmbR1 is a key transcriptional regulator for production of antifungal activity of *Burkholderia contaminans* strain MS14. *FEMS Microbiol. Lett. 297*, 54–60.
5. Ghannoum, M. G., and Rice, L. B. (1999) Antifungal agents: mode of action, mechanisms of resistance, and correlation of these mechanisms with bacterial resistance. *Clin. Microbiol. Rev. 12*, 501–517.
6. Kavanagh, K. (2007) New Insights in Medical Mycology , Springer, New York, NY.
7. Lorian, V. (2005), Antibiotics in Laboratory Medicine , Lippincott Williams & Wilkins, Philadelphia, PA.
8. Denning, D. W. (2002) Echinocandins: a new class of antifungal. *J. Antimicrob. Chemother. 49*, 889–891.
9. Ikeda, F., Tanaka, S., Ohki, H., Matsumoto, S., Maki, K., Katashima, M., Barrett, D., and Aoki, Y. (2007) Role of micafungin in the antifungal armamentarium. *Curr. Medic. Chem. 14*, 1263–1275.
10. de Groot, P. W. J., de Boer, A. D., Cunningham, J., Dekker, H. L., de Jong, L., Hellingwerf, K. J., de Koster, C., and Klis, F. M. (2004) Proteomic analysis of *Candida albicans* cell walls reveals covalently bound carbohydrate-active enzymes and adhesins. *Eukaryot. Cell 3*, 955–965.
11. Klis, F. M., de Groot, P., and Hellingwerf, K. (2001) Molecular organisation of the cell wall of *Candida albicans*. *Med. Mycol. 39*, 1–8.
12. Munro, C. A., and Gow, N. A. R. (2001) Chitin synthesis in human pathogenic fungi. *Med. Mycol. 39*, 41–53.
13. Roncero, C. (2002) The genetic complexity of chitin synthesis in fungi. *Curr. Genet. 41*, 367–378.
14. Douglas, C. M., D'Ippolito, J. A., Shei, G. J., Meinz, M., Onishi, J., Marrinan, J. A., Li, W., Abruzzo, G. K., Flattery, A., Bartizal, K., Mitchell, A., and Kurtz, M. B. (1997) Identification of the FKS1 gene of *Candida albicans* as the essential target of 1,3-β-D-glucan synthase inhibitors. *Antimicrob. Agents Chemother. 41*, 2471–2479.
15. Chiarini, L., Bevivino, A., Dalmastri, C., Tabacchioni, S., and Visca, P. (2006) *Burkholderia cepacia* complex species: health hazards and biotechnological potential. *Trends Microbiol. 14*, 277–286.
16. Mahenthiralingam, E., Baldwin, A., and Dowson, C. G. (2008) *Burkholderia cepacia* complex bacteria: opportunistic pathogens with important natural biology. *J. Appl. Microbiol. 104*, 1539–1551.
17. Walker, L. A., Munro, C. A., de Bruijn, I., Lenardon, M. D., McKinnon, A., and Gow, N. A. R. (2008) Stimulation of chitin synthesis rescues *Candida albicans* from echinocandins. *PloS Pathog. 4* (4), e1000040.
18. Nishiyama, Y., Hasumi, Y., Ueda, K., Uchida, K., and Yamaguchi, H. (2005) Effects of micafungin on the morphology of *Aspergillus fumigatus*. *J. Electron Microsc. 54*, 67–77.
19. Nakai, T., Hatano, K., Ikeda, F., and Shibuya, K. (2005) Electron microscopic findings for micafungin-treated experimental pulmonary aspergillosis in mice. *Med. Mycol. 43*, 439–445.
20. Angiolella, L., Maras, B., Stringaro, A. R., Arancia, G., Mondello, F., Girolamo, A., Palamara, A. T., and Cassone, A. (2005) Glucan-associated protein modulations and ultrastructural changes of the cell wall in *Candida albicans* treated with micafungin, a water-soluble, lipopeptide antimycotic. *J. Chemother. 17*, 409–416.
21. Tomana, M., Prchal, J., Garner, L., Skalka, H., and Barker, S. (1984) Gas chromatographic analysis of lens monosaccharides. *J. Lab. Clin. Med. 103*, 137–142.
22. Renfrow, M. B., Cooper, H. J., Tomana, M., Kulhavy, R., Hiki, Y., Toma, K., Emmett, M. R., Mestecky, J., Marshal, A. G., and Novak, J. (2005) Determination of aberrant *O*-glycosylation in the IgA1 hinge region by electron capture dissociation Fourier transform-ion cyclotron resonance mass spectrometry. *J. Biol. Chem. 280*, 19136–19145.
23. Wüthrich, K. (1986) NMR of Proteins and Nucleic Acids , Wiley, New York.
24. Braunschweiler, L., and Ernst, R. R. (1983) Coherence transfer by isotropic mixing - application to proton correlation spectroscopy. *J. Magn. Reson. 53*, 521–528.
25. Kumar, A., Ernst, R. R., and Wuthrich, K. (1980) A two-dimensional nuclear Overhauser enhancement (2D NOE) experiment for the elucidation of complete proton-proton cross-relaxation networks in biological macromolecules. *Biochem. Biophys. Res. Commun. 95*, 1–6.
26. Bothner-By, A. A., Stephens, R. L., Lee, J., Warren, C. D., and Jeanloz, R. W. (1984) Structure determination of a tetrasaccharide: transient nuclear Overhauser effects in the rotating frame. *J. Am. Chem. Soc. 106*, 811–813.
27. Bodenhausen, G., and Ruben, D. J. (1980) Natural abundance nitrogen-15 NMR by enhanced heteronuclear spectroscopy. *Chem. Phys. Lett. 69*, 185–188.
28. Hwang, T. L., and Shaka, A. J. (1995) Water suppression that works. Excitation sculpting using arbitrary waveforms and pulsed field gradients. *J. Magn. Reson. A112*, 275–279.
29. Dalvit, C. (1998) Efficient multiple-solvent suppression for the study of the interactions of organic solvents with biomolecules. *J. Biomol. NMR. SL1* 437–444.
30. Shaka, A. J., Lee, C. J., and Pines, A. (1988) Iterative schemes for bilinear operators - application to spin decoupling. *J. Magn. Reson. 77*, 274–293.
31. Marion, D., Ikura, M., Tschudin, R., and Bax, A. (1989) Rapid recording of 2D NMR-spectra without phase cycling - application to the study of hydrogen-exchange in proteins. *J. Magn. Reson. 85*, 393–399.
32. Kay, L. E., Keiffer, P., and Saarinen, T. (1992) Pure absorption gradient enhanced heteronuclear single quantum correlation spectroscopy with improved sensitivity. *J. Am. Chem. Soc. 114*, 10663–10665.
33. Boban, J. K., Plant, D., and Hurd, R. E. (1992) Improved proton-detected heteronuclear correlation using gradient-enhanced z and zz filters. *J. Magn. Reson. A101*, 113.
34. Delaglio, F., Grzesiek, S., Vuister, G. W., Zhu, G., Pfeifer, J., and Bax, A. (1995) NMRpipe - a multidimensional spectral processing system based on Unix pipes. *J. Biomol. NMR 6*, 277–293.
35. Johnson, B. A., and Blevins, R. A. (1994) NMRView - a Computer-Program for the Visualization and Analysis of NMR Data. *J. Biomol. NMR 4*, 603–614.
36. Gross, D., and DeVay, J. (1977) Production and purification of syringomycin, a phytotoxin produced by *Pseudomonas syringae*. *Physiol. Plant Pathol. 11*, 13–28.
37. Nishiyama, Y., Uchida, K., and Yamaguchi, H. (2002) Morphological changes of *Candida albicans* induced by micafungin (FK463), a water-soluble echinocandin-like lipopeptide. *J. Electron Microsc. 51*, 247–255.
38. Lin, S., Liehr, S., Cooperman, B. S., and Cotter, R. J. (2001) Sequencing cyclic peptide inhibitors of mammalian ribonucleotide reductase by electrospray ionization mass spectrometry. *J. Mass. Spectrom. 36*, 658–663.
39. Frias, H. V., Mendes, M. A., Cardozo, K. H. M., Carvalho, V. M., Tomazela, D., Colepicolo, P., and Pinto, E. (2006) Use of electrospray tandem mass spectrometry for identification of microcystins during a cyanobacterial bloom event. *Biochem. Biophys. Res. Commun. 344*, 741–746.
40. Felnagle, E. A., Jackson, E. E., Chan, Y. A., Podevels, A. M., Berti, A. D., McMahon, M. D., and Thomas, M. G. (2008) Nonribosomal

peptide synthetases involved in the production of medically relevant natural products. *Mol. Pharm. 5*, 191–211.
41. Waelder, S., Lee, L., and Redfield, A. G. (1975) Nuclear magnetic resonance studies of exchangeable protons. I. Fourier transform saturation-recovery and transfer of saturation of the tryptophan indole nitrogen proton. *J. Am. Chem. Soc. 97*, 2927–2928.
42. Krishnan-Natesan, S., and Chandrasekar, P. H. (2008) Current and future therapeutic options in the management of invasive aspergillosis. *Drugs 68*, 265–282.
43. Ngwogu, A. C., and Otokunefor, T. V. (2007) Epidemiology of dermatophytoses in a rural community in Eastern Nigeria and review of literature from Africa. *Mycopathologia 164*, 149–158.
44. Yaghmour, M. A., Inderbitzin, P., Bostock, R. M., and Michailides, T. J. (2008) Characterization of *Geotrichum candidum* causing sour rot of peaches and nectarines in California. *Phytopathology 98*, S175–S175.
45. Sfakianakis, A., Krasagakis, K., Stefanidou, M., Maraki, S., Koutsopoulos, A., Kofteridis, D., Samonis, G., and Tosca, A. (2007) Invasive cutaneous infection with *Geotrichum candidum* - sequential treatment with amphotericin B and voriconazole. *Med. Mycol. 45*, 81–84.
46. Pereira, D. I. B., Santurio, J. M., Alves, S. H., Argenta, J. S., Potter, L., Spanamberg, A., and Ferreiro, L. (2007) Caspofungin *in vitro* and *in vivo* activity against Brazilian *Pythium insidiosum* strains isolated from animals. *J. Antimicrob. Chemother. 60*, 1168–1171.
47. Argenta, J. S., Santurio, J. M., Alves, S. H., Pereira, D. I. B., Cavalheiro, A. S., Spanamberg, A., and Ferreiro, L. (2008) *In vitro* activities of voriconazole, itraconazole, and terbinafine alone or in combination against *Pythium insidiosum* isolates from Brazil. *Antimicrob. Agents Chemother. 52*, 767–769.
48. Popolo, L., Gualtieri, T., and Ragni, E. (2001) The yeast cell-wall salvage pathway. *Med. Mycol. 39*, 111–121.
49. Levin, D. E. (2005) Cell wall integrity signaling in *Saccharomyces cerevisiae*. *Microbiol. Mol. Biol.Rev. 69*, 262–291.
50. Douglas, C. M. (2001) Fungal β(1,3)-D-glucan synthesis. *Med. Mycol. 39*, 55–66.